Proceedings 10th NUMGE 2023
10th European Conference on Numerical Methods in Geotechnical Engineering
Zdravkovic L, Kontoe S, Taborda DMG, Tsiampousi A (eds)

https://doi.org/10.53243/NUMGE2023-105

Ultimate limit state design of deep excavation problems according to EC7 using numerical methods

H.-P. Daxer[1], H.F. Schweiger[1], F. Tschuchnigg[1]

[1]*Institute of Soil Mechanics, Foundation Engineering and Computational Geotechnics, Graz University of Technology, Graz, AUT*

ABSTRACT: For complex geotechnical problems, the finite element method (FEM) can be considered state-of-the-art with respect to the prediction of deformations and stresses for serviceability limit states (SLS). The verification of the ultimate limit state (ULS), on the other hand, is usually done using conventional methods. However, numerical methods are gaining relevance in the ULS design of geotechnical structures, which will also be reflected in the next generation of Eurocode 7 (EC7). Therefore, the design approaches used in EC7 require a detailed investigation on the factors influencing the design with numerical methods. In this paper, the design approaches DA2* and DA3 of EC7 are applied to a multi-strutted deep excavation problem using the Hardening Soil Small (HSS) and Mohr-Coulomb (MC) constitutive models. The differences resulting from the various design approaches and constitutive soil models are discussed. Since soil stiffness is known to play an important role in numerical analyses and its parameters are subject to a higher degree of uncertainty compared to strength parameters, it is shown that soil stiffness can have a major impact on the ULS design and the variation of its parameters can lead to significantly different results.

Keywords: Eurocode 7; Ultimate limit state; Numerical methods; Finite element method; Deep excavations

1 INTRODUCTION

The FEM is routinely used to assess the SLS of geotechnical structures, but the ULS is usually verified by means of conventional (analytical) methods. However, numerical methods are gaining importance also for the ULS design. On one hand, this is reflected in an increase in publications over the past 20 years (e.g. Simpson and Junaideen, 2013; Schweiger, 2014; Yeow, 2019). On the other hand, the new generation of EC7 (prEN 1997-1, 2021) will increasingly rely on the application of numerical methods. In order to identify and quantify factors that may influence the ULS design with numerical methods, the design approaches currently used within EC7 (EN 1997-1, 2013) must therefore be investigated in detail.

In this paper, the design approaches DA2* and DA3 (see section 2) are applied to a multi-strutted deep excavation (Schweiger, 2017). Both the HSS model (Schanz, 1998; Benz, 2007) and a linear elastic – perfectly plastic model with a MC failure criterion are used. Attention is paid to the differences in the design strut forces and the design bending moments of the retaining structure resulting from the various design approaches and the different constitutive models used. Moreover, it is shown, that the stiffness parameters can have a significant influence on the ULS design of deep excavations. All finite element analyses shown in this paper were conducted with PLAXIS 2D, CONNECT Edition V21.01 (Brinkgreve et al., 2021).

2 DESIGN APPROACHES ACCORDING TO EC7

In the current generation of EC7 (EN 1997-1, 2013), the three design approaches DA1, DA2 and DA3 are defined, whereby the design approach to be used is specified within the respective national annex. These three approaches differ in the way partial factors are applied to actions (or effects of actions), soil parameters and resistances. However, not all design approaches are readily applicable when using numerical methods such as the FEM. For example, DA2 requires permanent unfavourable actions to be factored by the partial factor γ_G, which may not be possible when using numerical methods. By applying the partial factor to the effects of actions (e.g. strut forces, bending moments) rather than to the actions (e.g. earth pressure), it is possible to account for the partial factor in numerical analyses. In this case, the design approach is referred to as DA2* (Bauduin et al., 2003). DA3 can be implemented using numerical methods in a straightforward manner, but the question arises at which stage of the analysis the partial factors on the soil strength parameters should be applied. In this regard, two methods can be distinguished. In method 1 (DA3-1), the finite element analysis is performed with characteristic soil parameters. Subsequently, the soil strength parameters are reduced to their design values by means of a φ/c-reduction (e.g. Zienkiewicz et al.,

1975; Griffiths and Lane, 1999) in relevant calculation phases. In method 2 (DA3-2), on the other hand, the soil strength parameters are already reduced from the very beginning of the analysis. When comparing both methods, it is apparent that DA3-1 offers the advantage of providing both SLS and ULS verifications within a single analysis.

3 NUMERICAL ANALYSES

3.1 Problem description

Figure 1 shows the investigated geometry of the multi-strutted deep excavation with an excavation depth of 17.00 m and a (half) width of 9.00 m. The excavation is supported by a 0.80 m thick diaphragm wall with a height of 28.00 m, of which 11.00 m are embedded in the subsoil below the excavation bottom. Three soil layers, namely "Fine sand", "Seeton 1" and "Seeton 2" are present, with the groundwater table at -3.40 m below the ground surface. Such soil stratification is typical for postglacially filled basins in alpine regions, with the "Seeton" mainly composed of silty fine sand in the upper part to clayey silt with thin fine sand layers in the lower part (Ausweger et al., 2019). During the five excavation stages, four rows of struts are installed.

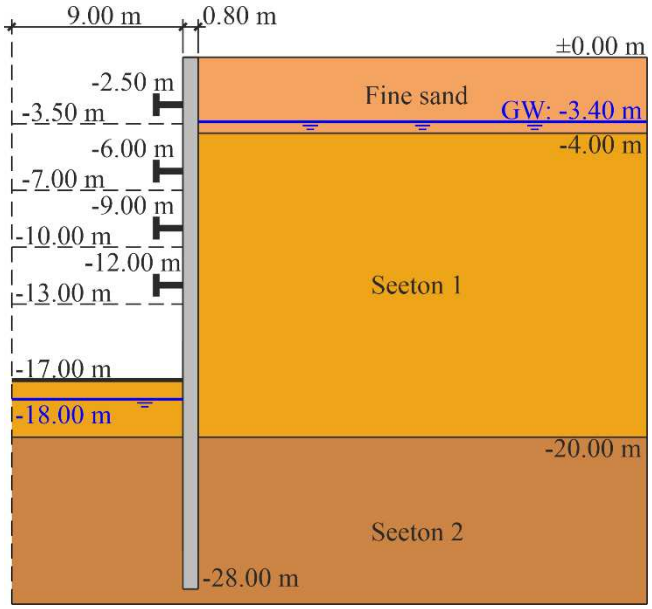

Figure 1. Geometry of the multi-strutted deep excavation

3.2 Parameters

Table 1 shows the soil parameters of the HSS model (the upper "Fine Sand" layer is modelled by means of the Hardening Soil (HS) model without small strain stiffness). While the HS model accounts for a stress-dependent stiffness in primary triaxial/oedometric loading (E_{50}^{ref}/ E_{oed}^{ref}) and un/reloading (E_{ur}^{ref}), the HSS model additionaly accounts for a high stiffness at very small strains ($\gamma_{0.7}$, G_0^{ref}). Moreover, Table 1 shows the unsaturated and saturated unit weights (γ_{unsat}, γ_{sat}), the power index (m), the strength parameters (c'_{ref}, φ' and ψ), the un/reloading Poisson's ratio (ν'_{ur}), the reference pressure for the stiffness moduli (p_{ref}), the coefficient of earth pressure at rest for normal consolidation (K_0^{nc}), the horizontal and vertical permeabilities (k_x, k_y), the interface strength reduction factor (R_{inter}), the coefficient of earth pressure at rest (K_0) and the overconsolidation ratio (OCR). The soil layers "Seeton 1" and "Seeton 2" are defined as undrained materials.

To (approximately) account for the stress-dependent stiffness with the MC constitutive model, the "Seeton 2" layer is further subdivided into two layers ranging from 20 – 36 m and 36 – 60 m below the ground surface (see also Figure 3). Of course, this is an assumption that accounts to some extent for the inability of the MC model to account for stress-dependent stiffness. There is no "rule" for this and thus the higher order model is preferred by the authors. The MC model is used here only because it is the model addressed in EC7 for ULSs. Within the MC constitutive model, the constant stiffness parameter E' is calculated according to Equation (1) at a reference level in the middle of each soil layer. Accordingly, the MC stiffness parameter E' from the top soil layer to the bottom soil layer is 7 500, 78 000, 92 000 and 129 000 kN/m² in combination with a Poisson's ratio ν' of 0.30.

$$E' = \frac{E_{50}^{ref} + E_{ur}^{ref}}{2} \cdot \left(\frac{\sigma'_h}{p_{ref}}\right)^m \qquad (1)$$

where σ'_h are the horizontal effective stresses.

Table 1. Parameters of the HSS constitutive model

Parameter	Unit	Fine Sand	Seeton 1	Seeton 2
Model	-	HS	HSS	HSS
Drainage	-	Drained	Undr.	Undr.
γ_{unsat}, γ_{sat}	kN/m³	20.00	20.00	20.00
E_{50}^{ref}	kN/m²	3 000	35 000	25 000
E_{oed}^{ref}	kN/m²	3 000	35 000	20 000
E_{ur}^{ref}	kN/m²	12 000	140 000	100 000
m	-	0.00	0.70	0.70
c'_{ref}	kN/m²	5.00	2.00	10.00
φ'	°	28.00	30.00	28.00
ψ	°	0.00	0.00	0.00
$\gamma_{0.7}$	-	-	2.00E-4	2.00E-4
G_0^{ref}	kN/m²	-	175 000	125 000
ν'_{ur}	-	0.20	0.20	0.20
p_{ref}	kN/m²	40.00	100.00	100.00
K_0^{nc}	-	1-sinφ'	1-sinφ'	1-sinφ'
k_x	m/day	8.64E-1	4.32E-3	8.64E-4
k_y	m/day	8.64E-3	4.32E-4	8.64E-5
R_{inter}	-	0.70	0.67	0.67
K_0	-	0.55	0.55	0.55
OCR	-	1.00	1.00	1.00

In Table 2 and Table 3, the parameters of the diaphragm wall (axial rigidity EA_1, flexural rigidity EI, weight w, Poisson's ratio ν) and the four strut levels (axial rigidity EA, strut spacing $L_{spacing}$) are shown. These structural elements are modelled using an elastic plate element with interfaces on both sides and elastic fixed-end-anchors, respectively.

Table 2. Parameters of the diaphragm wall

Parameter	Unit	Diaphragm wall
Material type	-	Elastic
Isotropic	-	Yes
EA_1	kN/m	23.20E6
EI	kNm²/m	1 237 333
w	kN/m/m	4.00
ν	-	0.20

Table 3. Parameters of the four strut levels

Parameter	Unit	Strut 1	Strut 2/3	Strut 4
Material type	-	Elastic	Elastic	Elastic
EA	kN	3.234E6	10.668E6	5.334E6
$L_{spacing}$	m	3.00	3.00	3.00

3.3 Mesh discretisation

Figure 2 and Figure 3 show the mesh discretisations for both the HSS and MC constitutive models with 5247 and 5385 (15-noded) elements. The total model dimensions are 150.00 m in width and 60.00 m in height.

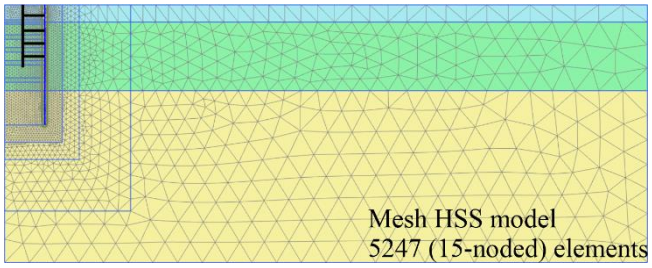

Figure 2. Mesh discretisation and soil layers HSS model

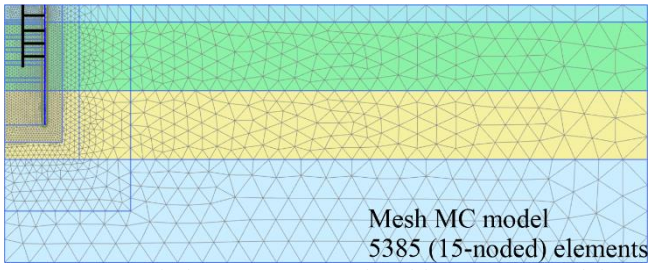

Figure 3. Mesh discretisation and soil layers MC model

3.4 Calculation phases

In total 22 calculation phases as shown in Table 4 are simulated. Within the initial phase, the initial stress field is modelled using the so-called K_0 procedure, i.e. the initial stress state is simply imposed on the stress points of the elements without any calculation. In the following, the diaphragm wall is activated (wished-in-place). This may lead to some inbalance of stresses and therefore a so-called plastic nil step is added in which any unbalance is resolved. Subsequently, the displacements (and small strains) are set to zero and the construction sequence is conducted. Within all groundwater lowering phases, the groundwater table within the excavation pit is lowered. to 1.00 m below the subsequent excavation level. In addition, undrained material behaviour (of "Seeton 1" and "Seeton 2") is ignored in these drawdown phases (and also for phases 1 and 2). This ensures that no excess pore water pressures are generated in groundwater lowering phases. For the given permeability it is not to be expected that significant groundwater flow is occuring during construction. Below the lowered groundwater table, the pore water pressure is interpolated down to -20.00 m (i.e. the transition zone between "Seeton 1" and "Seeton 2") for the calculation phases 3 – 14 (no groundwater flow analysis is performed). For the phases 15 – 21, the pore water pressure is interpolated down to -28.00 m (i.e. the base of the diaphragm wall). Soil clusters below the interpolation boundaries at -20.00 and -28.00 m are assigned to the initial groundwater table at -3.40 m outside of the excavation pit. Moreover, it should be mentioned that for all consolidation phases the time interval is set to 14 days as in the main publication (Schweiger, 2017). Therefore, the excess pore water pressure is by far not fully dissipated after the respective consolidation phase. It is not the aim here to investigate the consolidation behaviour during construction in detail but to compare the consequences of adopting the different design assumptions of EC7 for given assumptions.

Table 4. Calculation phases

#	Phase	To/At level [m]
0	Initial phase	
1	Diaphragm wall	
2	Plastic nil step	
3	1st GW lowering	-4.50
4	1st excavation	-3.50
5	1st strut level	-2.50
6	1st consolidation	
7	2nd GW lowering	-8.00
8	2nd excavation	-7.00
9	2nd strut level	-6.00
10	2nd consolidation	
11	3rd GW lowering	-11.00
12	3rd excavation	-10.00
13	3rd strut level	-9.00
14	3rd consolidation	
15	4th GW lowering	-14.00
16	4th excavation	-13.00
17	4th strut level	-12.00
18	4th consolidation	
19	5th GW lowering	-18.00
20	5th excavation	-17.00
21	5th consolidation	

4 RESULTS

In this section, the design approaches DA2*, DA3-1 and DA3-2 are applied to the multi-strutted deep excavation. When applying DA2*, all calculation phases are conducted with characteristic soil strength parameters. The partial factor for permanent unfavourable actions ($\gamma_G = 1.35$) is then applied to the strut forces and bending moments during the post processing of the analysis. Regarding DA3-1, new safety phases are introduced, starting from each of the characteristic calculation phases. Within these safety phases, the soil strength parameters are reduced to their design values ($FoS_{Target} = 1.25$) using the φ/c-reduction technique. For DA3-2, on the other hand, all calculation phases are conducted with design values of the soil strength parameters ($\gamma_\varphi = \gamma_c = 1.25$) from the outset of the analysis. While K_0 in this case is set to 0.55 for all soil layers, the parameter K_0^{nc} (when using the HS/HSS models) is calculated according to Jaky (1944) from the design value of the friction angle.

In the following, results for the (initial) stiffness parameters introduced in section 3.2 and for increased stiffness parameters are discussed. The latter represent analyses in which the stiffness parameters E_{50}^{ref}, E_{oed}^{ref}, E_{ur}^{ref} (HS/HSS models), G_0^{ref} (HSS model) and E' (MC model) are increased by 50%. In a parametric study, the stiffness has been increased and decreased in 10% steps but due to space limitations only the results for 50% are discussed in the following. The reason for this exercise is to draw attention to the influence of stiffness in such problems which is however not addressed in EC7 for ULS calculations. In these studies, the stiffness parameters (of all soil layers) are increased at the beginning of the analysis (K_0 procedure).

Figure 4 shows the bending moment envelopes M_{design} in combination with the initial (left) and increased stiffness parameters (right). While the deviations between the design approaches and constitutive models seem to be within an anticipated range when the initial stiffness parameters are applied (see also Table 5), significant deviations occur when the stiffness parameters are increased by 50% (see also Table 6). Especially for DA3-2 in combination with the HSS model (blue solid line), the bending moment envelope deviates significantly compared to DA2* (black solid line) and DA3-1 (red solid line). The deviations with respect to DA2* and DA3-1 are then in the order of -25.32% and -41.49% (-1401 kNm/m for DA2* vs. -1241 kNm/m for DA3-1 vs. -1756 kNm/m for DA3-2). In this case, however, the design bending moment changes from a negative to a positive sign. Thus, the minimum design bending moment of -1756 kNm/m given in Table 6 does not represent an absolute maximum value. When comparing the positive maximum values for the HSS model when the stiffness parameters are increased, DA3-2 deviates by -146.52% compared to DA3-1 (1018 kNm/m vs. 2509 kNm/m). With respect to the initial stiffness parameters, where the governing design approach changes depending on the constitutive model used, DA3-2 governs the design for the increased stiffness parameters in combination with both constitutive models. It is interesting to see that for DA2* the design bending moment decreases for increased soil stiffness as expected, but this is not the case for DA3 analyses.

Table 5. M_{design} for initial stiffness parameters

	M_{min} [kNm/m]	
Design approach	**HSS**	**MC**
DA2*	-1442	-1461
DA3-1	-1186	-1283
DA3-2	-1449	-1396

Table 6. M_{design} for 50% increased stiffness parameters

	M_{min} [kNm/m]	
Design approach	**HSS**	**MC**
DA2*	-1401	-1425
DA3-1	-1241	-1303
DA3-2	-1756	-1488

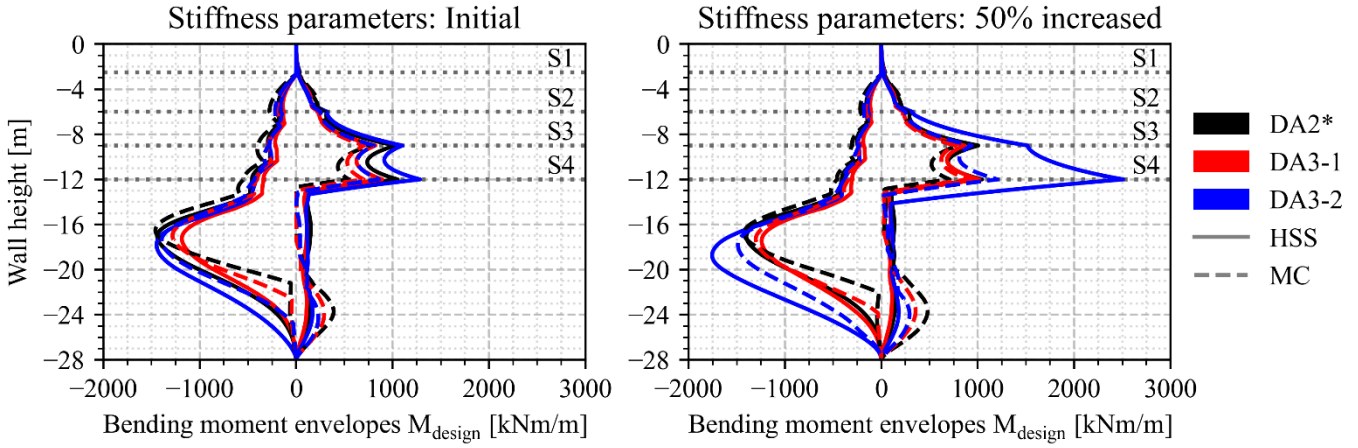

Figure 4. Bending moment envelopes M_{design}; left: initial stiffness parameters; right: 50% increased stiffness parameters

In Figure 5, the horizontal wall deflections u_x after the final consolidation phase are shown. It is worth mentioning that the wall deflections representing DA2* (solid and dashed black lines) are non-factored (i.e. characteristic) deformations. While for DA2* and DA3-1 the MC consitutive model leads to slightly larger (or similar) wall deflections, at least in the absolute maximum value, DA3-2 shows a completely different deformation behaviour (and also significantly larger deformations) in the area of the earth abutment when the HSS model is applied with increased stiffness parameters.

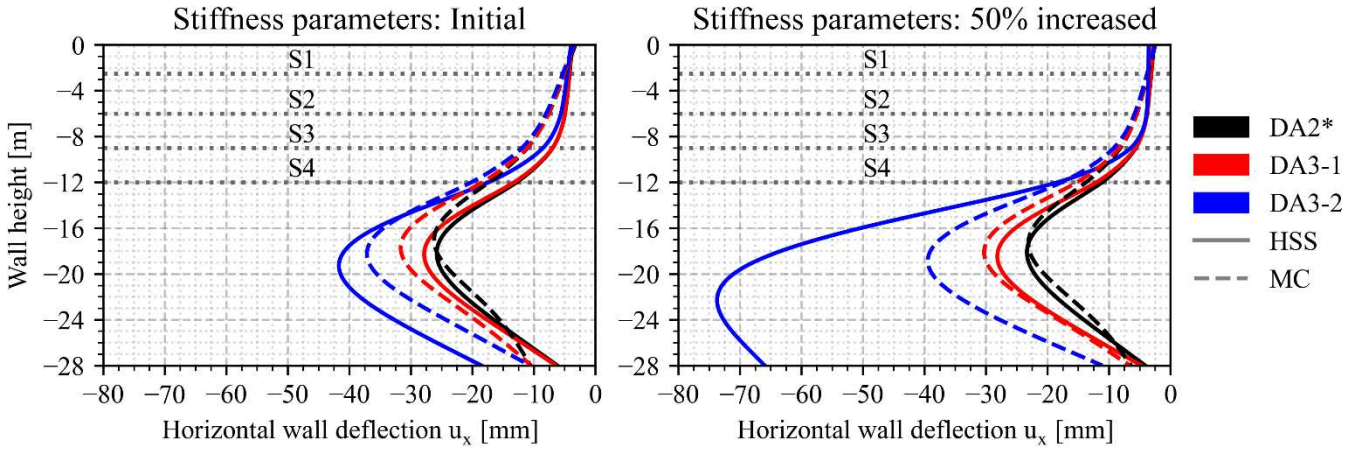

Figure 5. Horizontal wall deflections u_x; left: initial stiffness parameters; right: 50% increased stiffness parameters

The corresponding minimum (over all calculation phases) design strut forces F_{min} are shown in Figure 6. While DA2* governs the design of strut levels 1, 2 and 3 for both the initial and increased stiffness parameters, DA3-2 is governing the design of strut level 4. In Table 7, the minimum values for the increased stiffness parameters in combination with the HSS model are shown. The deviations with respect to DA2* appear to be relatively constant within strut levels 1, 2 and 3 for both DA3 approaches. Therefore, also the deviations between both DA3 approaches are almost constant at approximately -10% for these strut levels (e.g. -2325 kN for DA3-1 vs. -2540 kN for DA3-2 within strut level 3). However, within strut level 4, both DA3 approaches deviate significantly with -62.78% (-3786 kN for DA3-1 vs. -6163 kN for DA3-2) compared to each other.

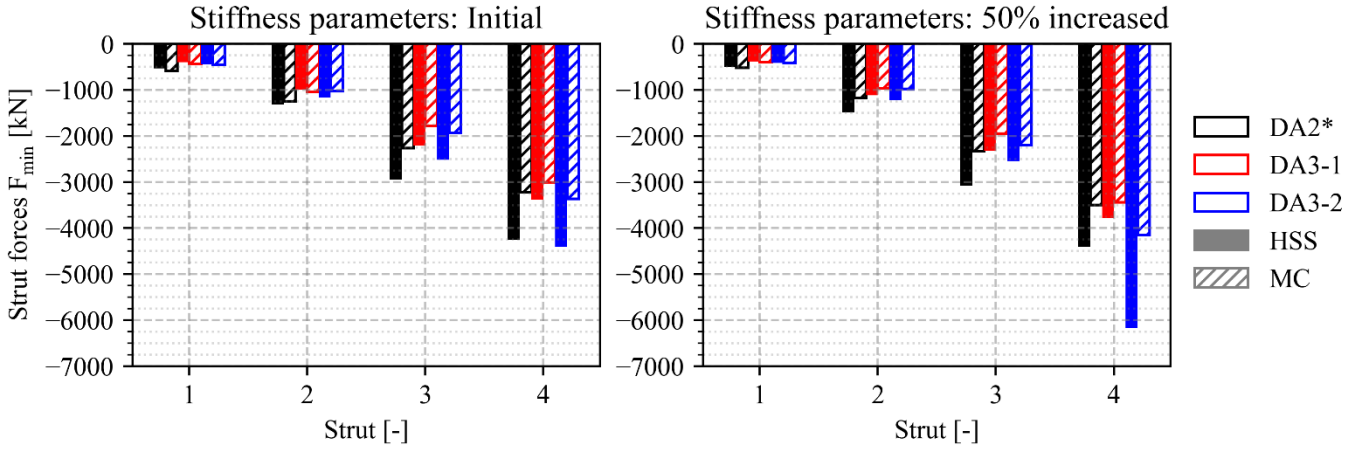

Figure 6. Design strut forces F_{min}; left: initial stiffness parameters; right: 50% increased stiffness parameters

Table 7. Design strut forces F_{min} for HSS model with 50% increased stiffness parameters

	F_{min} [kN]			
Design approach	**S1**	**S2**	**S3**	**S4**
DA2*	-495	-1484	-3076	-4405
DA3-1	-379	-1114	-2325	-3786
DA3-2	-415	-1220	-2540	-6163

Additional analyses are currently underway to identify the driving mechanisms for the significant differences for the two DA3 approaches in more detail. It is assumed that a key aspect is the soil stiffness, which is depending on the effective stresses for the HSS model and therefore the stiffness is very high at the final stage of excavation, because the excess pore water pressure is negative due to the excavation. However, near the excavation surface consolidation is fast and the negative excess pore water

pressure is quickly dissipating reducing effective stresses and as a consequence the stiffness. This effect is fully captured only in design approach DA3-2, which causes the significantly different behaviour. Figure 7 shows the earth pressure distributions for the HSS constitutive model with increased stiffness parameters for the penultimate (dashed lines) and the final (solid lines) construction stages. Again, the distributions representing DA2* show characteristic (non-factored) earth pressures. Regarding the 5th excavation stage, the earth pressure distributions show resulting forces on the active/passive side of the retaining structure of 2035 vs. 2078 for DA2*, 2017 vs. 2173 for DA3-1 and 2270 vs. 2141 kN/m for DA3-2. For the 5th consolidation phase, the resulting forces are 1939 vs. 1669 for DA2*, 1869 vs. 1789 for DA3-1 and 2251 vs. 1527 kN/m for DA3-2. Hence, for DA3-2, there is an excess in earth pressure of 724 kN/m on the active side. Nevertheless, with the pore water pressure on both sides of the retaining structure and the strut forces, equilibrium is achieved for all design approaches.

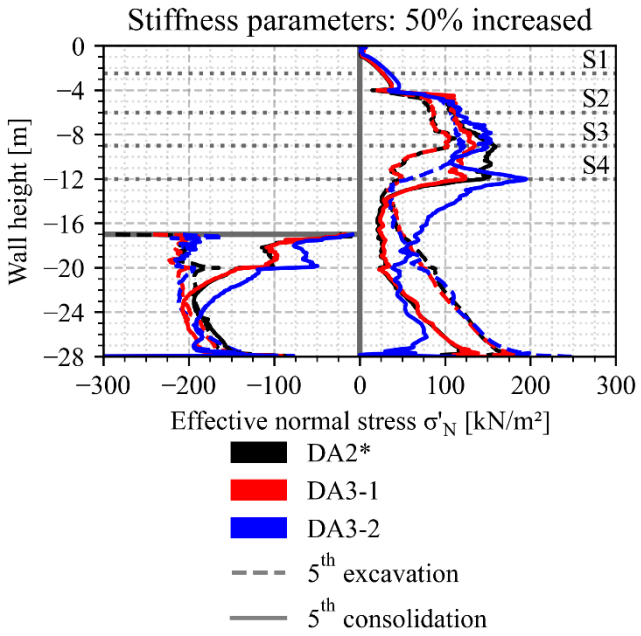

Figure 7. Earth pressure distributions for the HSS model with 50% increased stiffness parameters

5 CONCLUSIONS

In this paper, the design approaches DA2* and DA3 were applied to a multi-strutted deep excavation problem using the finite element method. While the differences between the various design appoaches appear to be negligible for relatively simple examples (e.g. Daxer et al., 2022), it was shown in this example that this cannot be generalised. Both investigated DA3 approaches can lead to significantly different results depending on the constitutive model and it seems that the soil stiffness may play a more pronounced role for more complex problems. To clearly identify the driving mechanisms for these differences, detailed analyses are currently in progress.

6 REFERENCES

Ausweger, G.M., Havinga, M., Lüftenegger, R., Marte, R., Oberhollenzer, S. 2019. Stiffness of Salzburger Seeton – Comparison of results from cone penetration tests and laboratory tests, *Geomechanics and Tunneling* **12(4)**, 328–339.

Bauduin, C., De Vos, M., Frank, R. 2003. ULS and SLS design of embedded walls according to Eurocode 7. *Proc. XIII ECSMGE* (Eds: Vaníček, I. et al.), 41-46. Czech Geotechnical Society, Prague.

Benz, T. 2007. Small-Strain Stiffness of Soils and ist Numerical Consequences. *Mitteilung 55 des Instituts für Geotechnik* (Ed: Vermeer, P.A.), Dissertation. University of Stuttgart, Stuttgart.

Brinkgreve, R.B.J., Kumarswamy, S., Swolfs, W.M., Fonseca, F., Ragi Manoj, N., Zampich, L., Zalamea, N. 2021. *PLAXIS 2D – CONNECT Edition V21.01 – Reference Manual*, Plaxis bv, Delft.

Daxer, H.-P., Tschuchnigg, F., Schweiger, H.F. 2022. Einflussfaktoren in der Nachweisführung nach EC7 mit numerischen Methoden am Beispiel einer tiefen Baugrube. *Workshop Numerische Methoden in der Geotechnik 2022* (Ed: Grabe, J.), 153-156. Hamburg University of Technology, Hamburg.

EN 1997-1:2004 (E) + AC:2009 + A1:2013 (E) 2013. *Eurocode 7: Geotechnical design – Part 1: General rules*, CEN, Brussels.

Griffiths, D.V., Lane, P.A. 1999. Slope stability analysis by finite elements, *Géotechnique* **49(3)**, 387–403.

Jaky, J. 1944. The coefficient of earth pressure at rest (In Hungarian (A nyugalmi nyomás tényezője), *Journal of the Society of Hungarian Architects and Engineers*, 355–358.

prEN 1997-1:20xx (E) 2021. *Eurocode 7: Geotechnical design – Part 1: General rules*, not published.

Schanz, T. 1998. Zur Modellierung des mechanischen Verhaltens von Reibungsmaterialien. *Mitteilung 45 des Instituts für Geotechnik* (Ed: Vermeer, P.A.), Habilitation. University of Stuttgart, Stuttgart.

Schweiger, H.F. 2014. Influence of EC7 design approaches on the design of deep excavation with FEM, *geotechnik* **37(3)**, 169–176.

Schweiger, H.F. 2017. Numerik in der geotechnischen Nachweisführung, *BAWMitteilungen* **101**, 87–96.

Simpson, B., Junaideen, S.M. 2013. Use of numerical analysis with Eurocode 7. *Proc. Int. Conf. Advances in Geotechnical Infrastructure* (Eds: Leung, C.F., Goh, S.H. & Shen, R.F.), 12pp. GeoSS, Singapore.

Yeow, H.-C. 2019. Ultimate Limit State Design Using FEM and Advanced Soil Model – A Case History of a 30 m Deep Excavation in London. *Geo-Congress 2019: Earth Retaining Structures and Geosynthetics* (Eds: Kumar, S., Pando, M.A. & Coe, J.T.), 68-81. ASCE, Philadelphia.

Zienkiewicz, O.C., Humpheson, C., Lewis, R.W. 1975. Associated and non-associated visco-plasticity and plasticity in soil mechanics, *Géotechnique* **25(4)**, 671–689.